Uniform growth of *fct* FePt nanoparticles on the surface of reduced-GO via a green facile approach. Ferromagnetic r-GO nanocomposites with high coercivity and surface area

Vasileios Tzitzios [a, b, f, *], Xiaocao Hu [c], Konstantinos Dimos [d], Dimitrios Gournis [d], Vasilios Georgakilas [e], George Avgouropoulos [e], Marios S. Katsiotis [f], Saeed M. Alhassan [f], George Hadjipanayis [b]

[a] Institute of Nanoscience and Nanotechnology, NCSR "Demokritos", 15310, Athens, Greece
[b] Department of Physics and Astronomy, University of Delaware, 217 Sharp Lab, Newark, DE, 19716, United States
[c] Department of Materials Science and Engineering, University of Delaware, Newark, DE, 19716, United States
[d] Department of Materials Science & Engineering, University of Ioannina, GR-45110, Ioannina, Greece
[e] Department of Materials Science, University of Patras, GR-26504, Rio Patras, Greece
[f] Department of Chemical Engineering, Khalifa University of Science and Technology, Petroleum Institute, P.O. Box 2533, Abu Dhabi, United Arab Emirates

ARTICLE INFO

ABSTRACT

FePt nanoparticles with the chemically ordered *fct* crystal structure have been widely studied because of the unique magnetic properties and the electrocatalytic activity for Oxygen Reduction Reactions (ORR). In this study, reduced graphene oxide (r-GO) supported FePt nanoparticles are successfully synthesized by a facile and completely green chemical approach. The structural, morphological, physicochemical and magnetic properties of the synthesized materials are systematically investigated by X-ray diffraction (XRD), Raman spectroscopy, X-ray photoelectron spectroscopy (XPS), transmission electron microscopy (TEM) and vibrating sample magnetometer (VSM) measurements. It is shown that the FePt nanoparticles with the *fct* crystal structure uniformly growth on the surface of the r-GO and remain isolated even after high temperature thermal treatment. Furthermore, the nanocomposite materials reveal strong ferromagnetic behavior at room temperature.

© 2017 Elsevier Ltd. All rights reserved.

1. Introduction

Last decade, there is a tremendous interest in the research community concerning the development of hybrid materials based on graphene or graphene oxides and inorganic materials from both the fundamental and technological point of view. Graphene sheets, a monolayer of carbon atoms with sp^2 hybridization and fully delocalized p-electrons, are attractive nanoscale building blocks for the creation of new materials, owed to their unique nanostructure and properties. Graphene oxide (GO), an oxygen rich derivative of graphene decorated with hydroxyl, epoxy, and carboxyl groups is created by strong oxidation of graphite. GO can be easily reduced to graphene (r-GO) by various methods including chemical, catalytic, plasma-induced, thermally induced and photo-induced reduction. A plethora of methodologies has been reported in the literature for the synthesis of inorganic nanoparticles/graphene composite materials including noble and precious metals [1–6], metal oxides [7–10] and non-metallic elements such as sulfur [11], and phosphorous [5,12]. Concerning the magnetic/graphene composites, the synthesis of Fe$_3$O$_4$/graphene composites for dye removal from aqueous media have been recently reported [13], as well as the synthesis of CoFe$_2$O$_4$/graphene via a traditional co-precipitation procedure and tested for the catalytic decomposition of organic pollutant [14]. Furthermore, the decoration of graphene and graphene oxides with bimetallic magnetic particles like FeCo [15,16] and FePt [17–21] has been reported mainly for catalytic application in oxygen reduction reactions (ORR) and for biomedical application like dual modal imaging and potential theranostic platforms [22].

---

* Corresponding author. Institute of Nanoscience and Nanotechnology, NCSR "Demokritos", 15310, Athens, Greece.
E-mail addresses: v.tzitzios@inn.demokritos.gr, vatzitzios@pi.ac.ae (V. Tzitzios).

Considering the procedures for the synthesis of FePt/r-GO nanocomposites, Guo and Sun [17] followed a self-assembly methodology of pre-synthesized *fcc*-FePt nanoparticles on GO reduced by a DMF methodology, while Chen et al. [18] following a solvothermal polyol method decorated and simultaneously reduced GO with *fcc*-FePt nanoparticles. Hydrazine [19] and NaBH$_4$ [20] reduction methods have also been reported, leading to 4–6 nm *fcc*-FePt particles on the surface of r-GO [19]. The main interest concerning these particular nanocomposites arise from the enhanced electrocatalytic activity and durability compared with the traditional Pt based electrocatalysts [17]. Additionally, among the *fcc* and *fct* FePt crystal structures the *fct*-FePt appears to be more active and durable than the *fcc*-FePt due to its more stable inter-metallic Fe and Pt arrangement [23]. It is also worth to mention the synthesis of *fct* FePt nanoparticles in the interior space of multiwall carbon nanotubes using the [Fe(H$_2$O)$_6$][PtCl$_6$] complex as metals precursor [24].

Here we demonstrate a facile green approach for the decoration of reduced GO by FePt nanoparticles in both the *fcc* and *fct* crystal structure. The method involves the use only of the appropriate inorganic salts (FeCl$_2$, H$_2$PtCl$_6$·xH$_2$O), graphene oxide and water. A simple solid state annealing method is followed, compared with other liquid phase procedures where toxic and generally dangerous reagents such as Fe(CO)$_5$, organic solvents (octyl ether, DMF) and strong reducing agents (NaBH$_4$, hydrazine) are used, this methodology is very safe, more economic and poses no significant environmental risks. The composite materials reveal strong ferromagnetic behavior and one of the highest specific surface area reported in the literature. The main achievement presented herein is the decoration of an organic layered material (GO) with a layered bimetallic molecular precursor ([Fe(H$_2$O)$_6$][PtCl$_6$] complex) and the formation of the *fct*-FePt nanoparticles directly on the surface of the exfoliated r-GO via a simple thermal annealing.

2. Experimental

2.1. Materials and methods

The synthesis of FePt/r-GO nanohybrids was based on the decoration of exfoliated GO by the layered bimetallic [Fe(H$_2$O)$_6$] PtCl$_6$ complex in water. On a typical procedure, 40 mg of GO were exfoliated in 100 ml of H$_2$O by high power probe sonication. The saline [Fe(H$_2$O)$_6$]PtCl$_6$ complex was synthesized according to the literature [25,26] by reacting equimolecular amounts of FeCl$_2$·4H$_2$O and H$_2$PtCl$_6$·6H$_2$O and keeping the pH ~ 1 to prevent the Fe^{2+} to Fe^{3+} oxidation. The [Fe(H$_2$O)$_6$][PtCl$_6$] aqueous solution was then added dropwise and under continued sonication to the aqueous GO dispersion. The [Fe(H$_2$O)$_6$]PtCl$_6$/GO dispersion was left to precipitate and the solid material was collected by filtration, leaving a clear and colorless supernatant that indication the quantitative sorption of the binuclear complex on the GO surface, and dried over-night at room temperature. The XRD diffraction patterns from the GO, the binuclear complex and the binuclear complex/GO composite are presented in Fig. 1S in the supplementary section. The pristine GO sample shows a sharp peak at $2\theta = 11.9°$ corresponded to the (001) reflection of GO. However, the characteristic peak of the GO cannot be observed in the XRD pattern of the binuclear complex/GO composite sample indicating the exfoliation of the GO after the sorption of the [Fe(H$_2$O)$_6$]PtCl$_6$. On the other hand, there is an obvious crystal structure transformation of the layered [Fe(H$_2$O)$_6$] PtCl$_6$ after the interaction with the GO surface. This is probably due to the interaction between the complex and the functional groups of the GO like COOH and OH. Nevertheless, the inorganic salt re-mains in a crystalline form after the deposition on the GO surface leading to the formation of equiatomic FePt nanoparticles after the

annealing procedure as presented in the results below.

It is well known from literature that the thermal decomposition of the above bimetallic complex leads to the formation of the *fct*-FePt material even after treatment at 400 °C [27,28]. Finally, the hybrid Fe-Pt binuclear complex/GO material was annealed at elevated temperature (500–950 °C for 30 min) under reducing atmosphere, forming gas (5% H$_2$ in Ar), in order to decompose the inorganic precursor into FePt nanoparticles and simultaneously to reduce the GO to r-GO.

The experimental approach is schematically illustrated in Scheme 1. In order to investigate the role of the layered bimetallic complex a different synthetic pathway was followed using instead of the binuclear [Fe(H$_2$O)$_6$]PtCl$_6$ complex an equimolecular solution of FeCl$_2$ and H$_2$PtCl$_6$. After annealing the corresponding material at 500 °C the TEM measurements show clearly that the FePt nano-particles do not instead decorate uniformly the r-GO surface and have totally irregular morphology as presented in the Supporting Information section (Fig. 2S).

2.2. Materials characterization

In order to confirm the crystal structure of the FePt/r-GO nanocomposites X-ray diffraction (XRD), X-ray photoelectron spectroscopy (XPS) and Raman spectroscopy were used. Trans-mission electron microscopy (TEM, JEOL JEM-3010 at 300 keV voltage) measurements revealed the morphology and energy dispersion spectroscopy (EDS) analysis was applied to estimate the elemental content of the nanoparticles. Magnetic properties were measured with a vibrating sample magnetometer (3 T Versalab, Quantum Desing). Finally, nitrogen adsorption-desorption mea-surements were performed in order to estimate the surface area and the pore characteristics of the final hybrid product.

X-ray photoelectron spectroscopy (XPS) measurements were performed under ultrahigh vacuum conditions with a base pressure of 5×10^{-10} mbar in a SPECS GmbH instrument equipped with a monochromatic MgKα source ($h\nu = 1253.6$ eV) and a Phoibos-100 hemispherical analyzer. Pulverized samples were dispersed in toluene (1 wt %), and after short sonication and stirring, a minute quantity of the suspensions was drop cast on evaporated gold films supported on mica substrates and left to dry in air before transfer to ultrahigh vacuum. The energy resolution was set to 0.3 eV and the photoelectron take-off angle was 45° with respect to the surface normal. Recorded spectra were the average of 3 scans with energy step set to 0.05 eV and dwell time 1 s. All binding energies were referenced to the C1s core level at 284.6 eV. Spectral analysis included a Shirley background subtraction and peak deconvolution employing mixed Gaussian–Lorentzian functions, in a least squares curve-fitting program (WinSpec) developed at the Laboratoire Interdisciplinaire de Spectroscopie Electronique, University of Namur, Belgium.

Raman spectra were recorded with a micro-Raman (μ-Raman) Renishaw RM1000 system using a laser diode excitation line at 532 nm in the frequency range of 200–3500 cm^{-1}. Raman scatter was collected by means of an Olympus optical microscope, equip-ped with 50 × and 100 × lenses. Using the 50 × lens, the probing spot was about 2 μm in diameter, while laser was operated at 20 mW unless photodecomposition occurred and power was decreased. The spectrometer was calibrated by recording the spectrum from a Si sample with characteristic Raman peak at 520.7 cm^{-1}. Raman spectra were obtained from samples in the form of drop casted films onto glass substrates. The reported spectra are an average of 3–5 scans.

The specific surface area (S$_{BET}$), the pore volume (VP) and the pore size distribution of the sample were determined from the adsorption and desorption isotherms of nitrogen at -196 °C using a
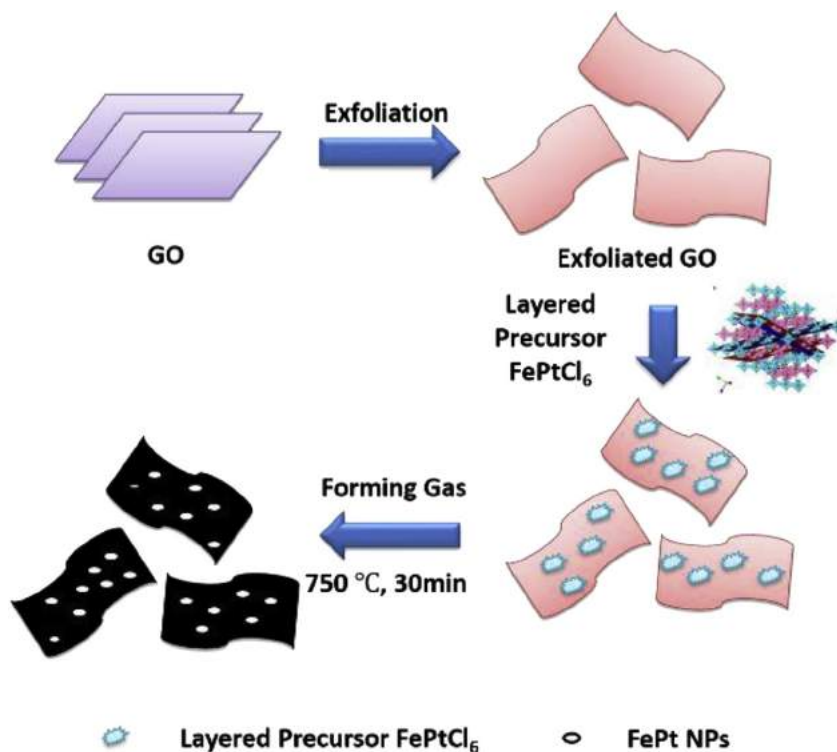
Scheme 1. Schematic illustration of the experimental procedure for the synthesis of FePt/r-GO nanocomposites through the interaction of a layered bimetallic inorganic complex and exfoliated GO.

Micromeritics Tristar 3000 instrument. The specific surface area (S_{BET}) of the sample was calculated following the BET (Brunauer—Emmett—Teller) procedure with six relative pressures of nitrogen in the range of 0.05—0.3. The Barret—Joyner—Halenda (BJH) method was used to determine pore size distribution, considering the desorption curves. Prior to the measurements, the samples were outgassed at 150 °C for 1.5 h under nitrogen flow.

3. Results and discussion

3.1. X-ray diffraction studies

The XRD patterns of FePt/r-GO nanohybrids annealed at 500—950 °C under 5% H_2 reducing atmosphere are presented in Fig. 1. After annealing at 500 °C three main diffraction peaks are observed, one intense peak around $2\theta = 24°$ which corresponds to the (002) diffraction plane of r-GO, while the other two peaks at 40° and 46.5° can be attributed to the (111) and (200) planes of the chemically disordered *fcc* FePt phase. The gradual development in the ordered *fct* (L1$_0$ type) phase of the FePt nanoparticles can be observed in the diffractograms with increasing annealing temperature. Specifically, the observed splitting of the (200) and (220) peaks is a characteristic mark of this transformation. In addition, the appearance of the (001) and (110) superlattice peaks in the low 2θ range is indicative of the high percentage of a chemically long-range ordered *fct* state. The evolution of the ordered *fct* FePt phase progresses with increasing annealing temperature. After annealing at 950 °C, the appearance of the (201) superlattice peak is obvious suggesting a higher degree of the *fcc* to *fct* transformation. Concerning the r-GO substrate, the intensity of the (002) diffraction peak decreases with increasing temperature; this can be possibly attributed to increasing particle size (as observed with TEM — see below), and the fact that the attached nanoparticles on the surface
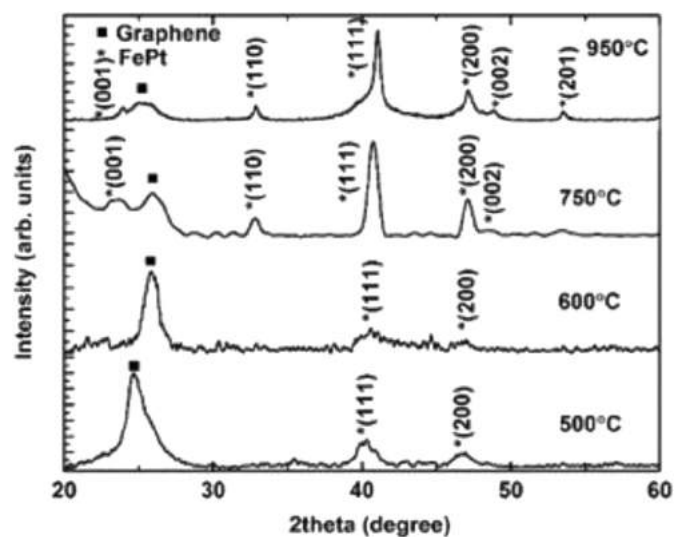

Fig. 1. X-ray diffraction patterns from FePt/r-GO nanocomposites after reductive annealing under 5% H_2 in Ar atmosphere at elevated temperatures (500 and 950 °C).

of the r-GO sheets prevent restacking [29].

3.2. Microscopy studies-morphological characterization

TEM and HR-EM images from the FePt/r-GO nanohybrids that were annealed between 500 and 950 °C are presented in Fig. 2, along with the size distribution analysis. In all cases it is clear that the bimetallic FePt nanoparticles decorate the surface of the r-GO sheets. The shape of the particles is almost spherical, while the size increases with increase of the annealing temperature. It should be
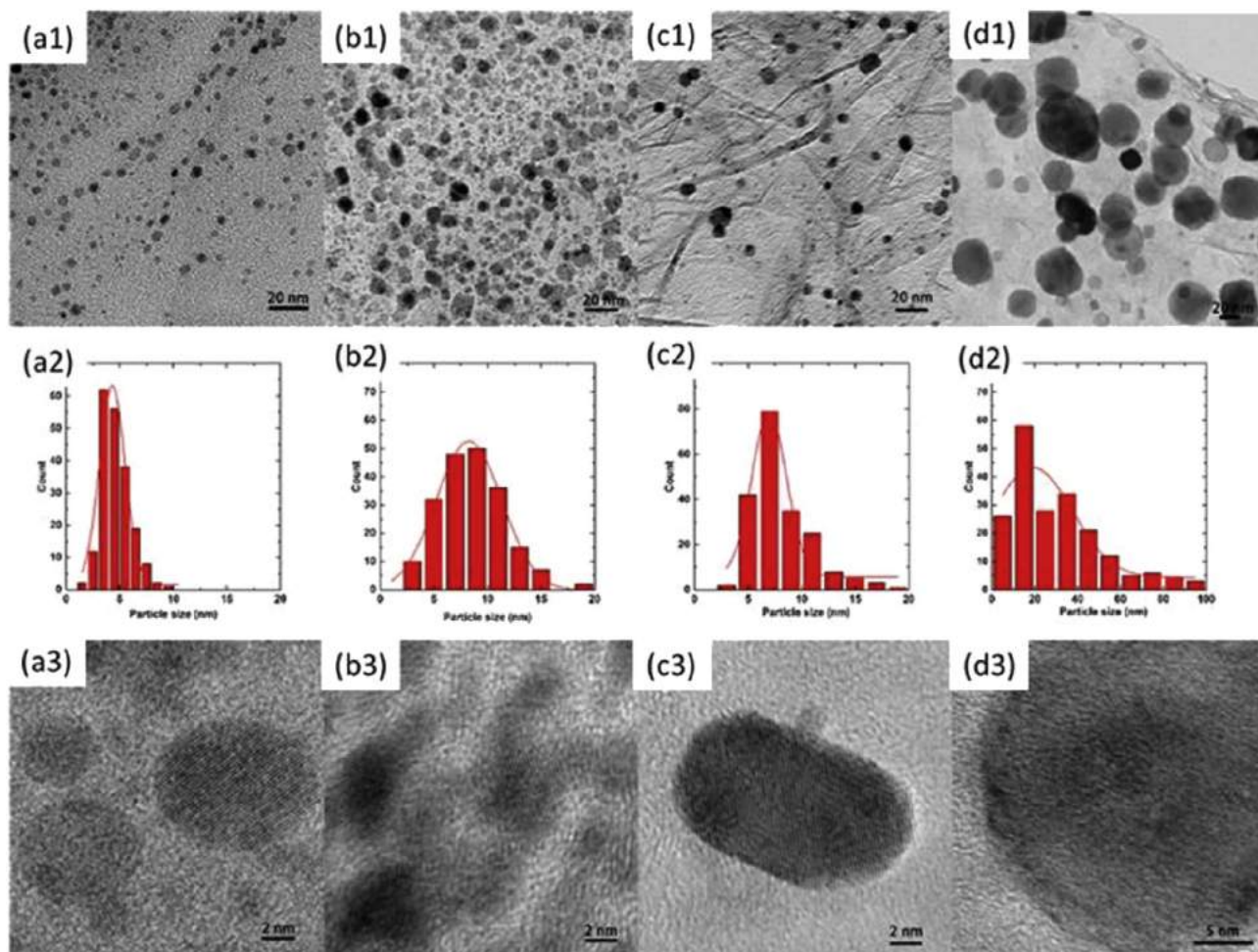
Fig. 2. TEM, HR-TEM and size distribution analysis of the FePt/r-GO nanohybrids after annealing under 5% H_2 in Ar atmosphere at 500 °C (a), 600 °C (b), 750 °C (c) and 950 °C (d) for 30 min. (A colour version of this figure can be viewed online.)

mentioned that even after annealing at 950 °C the inorganic material exhibits limited agglomeration and most importantly the particles remain isolated. A possible explanation for this "particle immobilization" on the surface of r-GO, is that the particles anchor themselves on the r-GO; thus, only neighboring particles are allowed to collapse and the uncontrollable aggregation that usually takes place in the FePt particles, at temperatures significantly lower than 950 °C, is not observed. The mean diameter of the FePt nanoparticles was measured to be 4.6 nm after annealing at 500 °C, 8.1 and 8.6 nm after annealing at 600 and 750 °C respectively; at 950 °C the size increased up to 29.8 nm.

TEM and EDS analysis of FePt/r-GO nanocomposites after annealing at 750 °C for 30 min is presented in Fig. 3. It is clear that even after the high temperature annealing the FePt particles remain completely isolated and uniformly distributed on the surface of the r-GO. The elemental atomic composition of the FePt particles is $Fe_{56}Pt_{44}$ according to EDS analysis which is in the range of the *fct* structure formation and very close to equiatomic ratio taking into account that the starting bimetallic $[Fe(H_2O)_6]PtCl_6$ complex is equimolecular.

3.3. XPS and Raman spectroscopies studies

Furthermore, the materials were characterized by XPS and Raman spectroscopies. C1s core level XPS spectrum and Raman spectrum of FePt/r-GO annealed at 750 °C are shown in Fig. 4.

Following deconvolution with mixed Gaussian–Lorentzian functions, the C1s spectrum consists of five components. The first component, recorded at a binding energy of 284.6 eV, corresponds to C–C and C–H bonds and contributes a 20.0% to the total C1s intensity. The main peak at 285.6 eV, representing 42.2% of the total C1s intensity, is attributed to hydroxyl C–O bonds, while the third peak at 286.5 eV (23.8%) is assigned to C–O–C epoxide/ether groups. The peak at 287.4 eV (11.7%) originates from the carbonyl functional groups (C=O), whereas the higher binding energy contribution located at 288.7 eV (2.3%) is associated with carboxyl groups (O–C=O) [30,31]. Shape and deconvolution of the C1s XPS spectrum strongly suggest that graphene oxide undergoes partial reduction upon annealing at 750 °C. This behavior is commonly found with thermal annealing in a reducing Ar/H_2 atmosphere [32]. Although oxygenated groups and mainly C–O still dominate the C1s spectrum, reduction is exposed by two facts: A noteworthy contribution from the C–C bonds arises at lower binding energy; in addition the shape of the spectrum exhibits visible differences compared to relevant C1s XPS spectra of pristine GO, where the C–C bond usually has minor contribution while more oxidized species dominated, such as carboxyl and carbonyl groups [30,33,34].

Raman spectrum of FePt/r-GO annealed at 750 °C exhibits both G- and D-bands at 1583 and 1349 cm^{-1} respectively. The G-band at 1583 cm^{-1} which is associated with sp^2 hybridized carbon atoms is asymmetric and shifted compared to the G-band of GO, near the relevant peak of graphite which is positioned at ~1580 cm^{-1} [35,36].
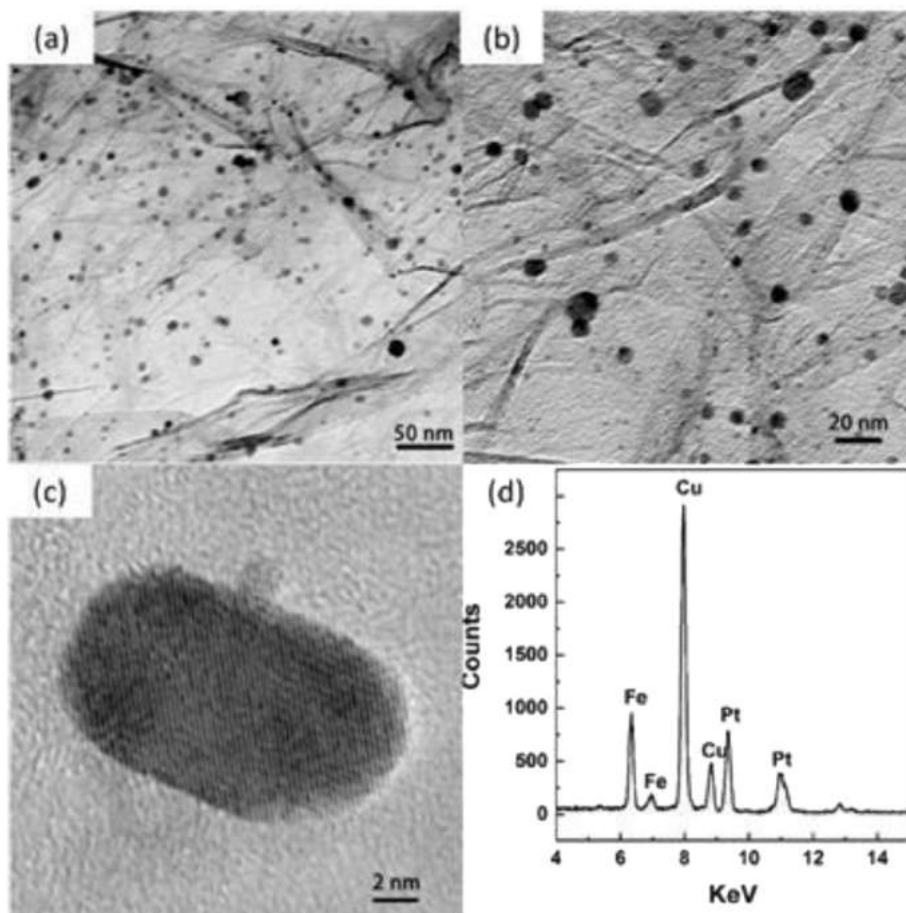
Fig. 3. TEM (a, b) HR-TEM (c) and EDAX analysis (d) of the FePt/r-GO nanocomposite annealed under 5% H_2 in Ar atmosphere at 750 °C for 30 min.
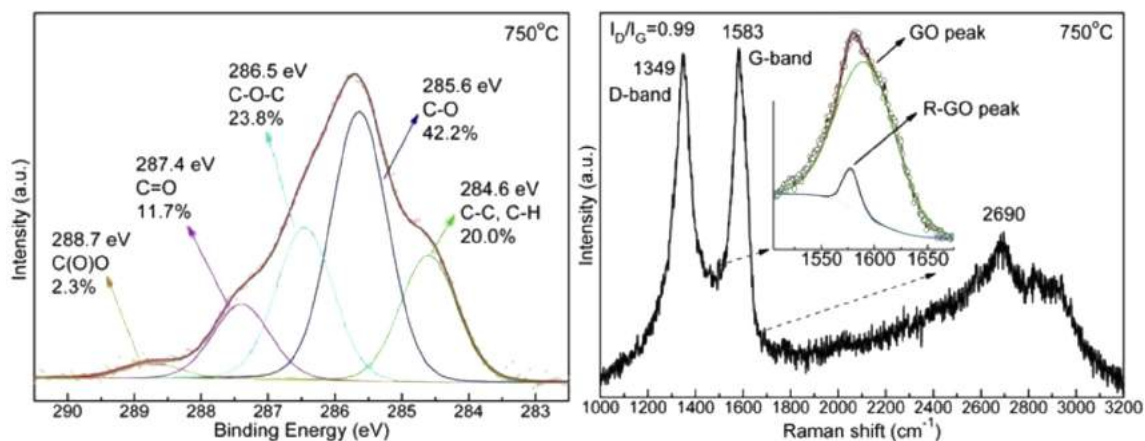

Fig. 4. (a) C1s core level X-ray photoemission spectrum of FePt/r-GO annealed at 750 °C and (b) Raman spectrum of FePt/r-GO annealed at 750 °C. Inset of (b): zoom in on the region of the G-band. (A colour version of this figure can be viewed online.)

As observed clearly in the inset of Fig. 4b, the G-band consists of two different peaks, the one derived by pristine GO at ~ 1600 cm^{-1} and a minor sharper one arising from reduced GO at ~ 1580 cm^{-1}. In addition, while GO does not have significant peaks in the 2D region [37,38], a broad peak arises at 2690 cm^{-1} in the Raman spectrum of the 750 °C annealed sample. This is ascribed to the 2D vibrational mode (overtone of the D peak) and has roughly half the intensity of the G-band [35,36]. According to literature, the red shift of G-band,

the enhanced intensity of the 2D peak as well as its shift below 2700 cm^{-1} are clear evidence of the r-GO presence with a few layers formation [30,35,39]. The exact number of stacked graphene layers cannot be estimated in this case; although thanks to the broadening of the 2D peak it is rational to expect a wide distribution concerning the number of the stacked layers.

Raman spectra of FePt/r-GO annealed at all four temperatures are presented in Fig. 5. As seen there, the D-band is recorded at

$1349\ cm^{-1}$ in all cases, whereas the G-band appears at $1593\ cm^{-1}$ except for the 750 °C sample as discussed previously. Moreover, samples that were annealed at 500 °C and 600 °C do not exhibit any important peak in the 2D region in contrary with the 750 °C annealed sample. These two observations, the position of the G-band and the lack of any major 2D peaks, suggest that the annealing process at the low temperature range 500–600 °C under the H_2/Ar reducing atmosphere did not lead to relevant reduction of GO as for the samples that were annealed at temperatures higher than 750 °C. This conclusion comes in full agreement with the XPS spectra (not shown here). Furthermore, the ratio of the D- to G-band intensities (I_D/I_G) is increasing with higher annealing temperatures. I_D/I_G is equal to 0.88 for the first two samples where the temperature variation is small, but reaches 0.99 for the FePt/r-GO annealed at 750 °C and 1.06 for the FePt/r-GO annealed at 950 °C. This is expected and well documented in the literature since together with the restoration of the sp^2 graphene lattice, defects and vacancies are also formed, while at the same time the full width at half maximum of the D-band decreases [32,34].

3.4. Surface area properties

For the FePt/r-GO sample annealed at 750 °C, the nitrogen adsorption/desorption isotherm is found to be of type II with a type B hysteresis loop, which is closed at P/P$_0$ values in the range of 0.40–0.50 (Fig. 6a). The pore size distribution, as estimated using the BJH method, indicates a mesoporous nature of the material with pores of various sizes starting from ~10 nm and extending well into the macropore region (Fig. 6b). A small distribution of micropores with a mean size of 2.5 nm is also present. The surface area (S_{BET}) of the FePt/r-GO nanohybrids is 1055 m^2/g and the pore volume is 6.43 cm^3/g. This specific surface area value is one of the highest among the values presented in the literature and varied from 400 to 700 m^2/g for GO that reduced by H_2 [40–42].

3.5. Magnetic properties studies

The magnetic properties of the corresponding materials were measured using a vibrating sample magnetometer (VSM) at room temperature. The room temperature magnetic hysteresis loops from the FePt/r-GO nanohybrids after annealing in the temperature
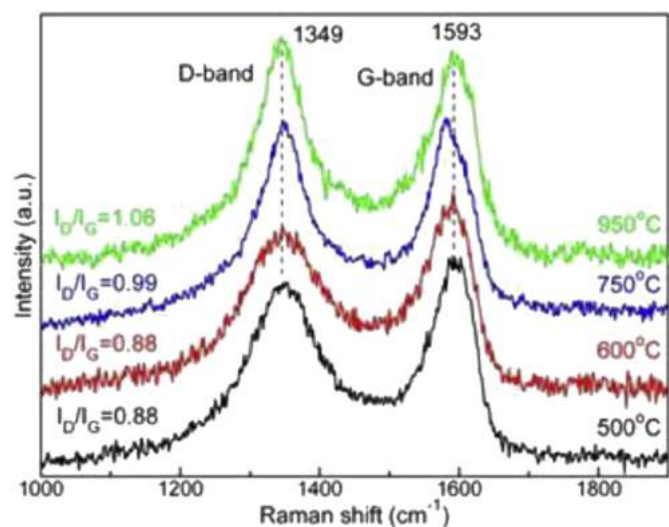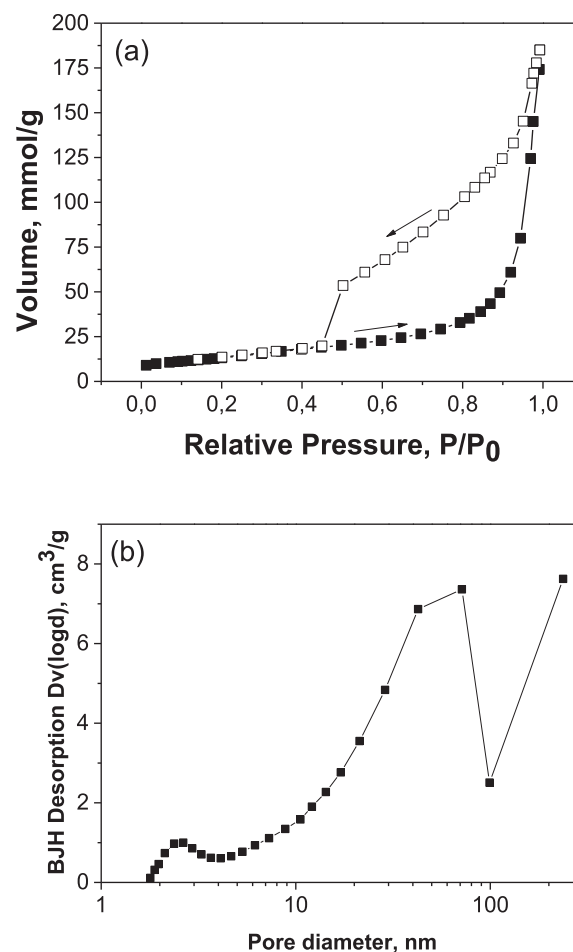
Fig. 6. Nitrogen adsorption/desorption isotherms (a) and pore size distribution (b) from the FePt/r-GO nanocomposite annealed at 750 °C. Adsorption (solid symbols)/ Desorption (open symbols).

range of 500–900 °C under 4% H_2-Ar gas mixture for 30 min are presented in Fig. 7. All materials reveal ferromagnetic behavior that also confirms the *fcc* to *fct* FePt transformation. After annealing at 500 °C the coercivity was quite low (0.4 kOe), while progressively increased at 4, 8.1 and 9.9 kOe after annealing at 600, 750 and 950 °C, respectively suggesting the evolution of the ordered *fct* FePt structure. Taking into account the coercivity evolution the *fct* ordering actually starts at 600 °C, temperature that is much higher than the published one for the *fcc* to *fct* transformation temperature of the layered [Fe(H$_2$O)$_6$][PtCl$_6$] complex which is 400–450 °C [27,28]. This almost 150 °C delay on the transformation temperature is probably due to the structural changes of the layered complex after the deposition on the GO surface. The saturation magnetization varied from 7.5 to 11.5 emu/g. The low saturation magnetization value arises from the low FePt loading in the final composites.

4. Conclusions

In summary, we demonstrate here a facile green chemical approach for the synthesis of *fct* FePt/r-GO nanohybrid materials combining a single binuclear layered molecular precursor and exfoliated GO. The synthetic method was based on the decoration of exfoliated GO with the layered bimetallic [Fe(H$_2$O)$_6$]PtCl$_6$ complex in an aqueous medium, followed by a solid state annealing procedure at elevated temperatures. The use of the bimetallic
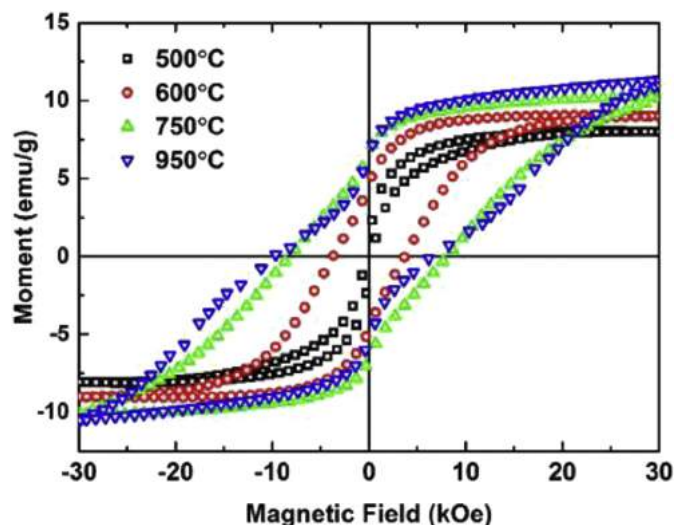
Fig. 5. Raman spectra of FePt/r-GO nanohybrids annealed at 500 °C, 600 °C, 750 °C and 950 °C under 5% H_2 in Ar atmosphere. (A colour version of this figure can be viewed online.)

Fig. 7. Room temperature magnetic hysteresis loops of FePt/r-GO nanohybrids after annealing at 500—950 °C under 5% H_2 in Ar atmosphere for 30 min. (A colour version of this figure can be viewed online.)

complex is very crucial for the uniform decoration of r-GO with isolated FePt nanoparticles. The annealing step results in the reductive decomposition of the inorganic iron/platinum complex and leads to the formation of bimetallic FePt nanoparticles in the ordered *fct* phase, and simultaneous reduction of GO. The composite materials exhibit one of the highest reported in the literature BET specific area value, (up to 1055 m^2/g). Furthermore, the immobilization of FePt nanoparticles on the surface of r-GO seems to protect them from uncontrollable sintering. The particles remain completely isolated even after annealing at 950 °C. It is also worth to mention, that the current methodology, because of the complete absence of any organic molecule as surfactant and/or solvent in the overall procedure, and the use of simple inorganic salts as metal precursors, lead to the formation of clean surface inorganic particles without any traces of carbon that actually blocks the catalytic active centres in many cases. It is well know that FePt in the ordered *fct* crystal structure is a very active electrocatalyst for oxygen reduction (ORR) [43—45], and methanol oxidation reactions [46]. Work is in progress concerning the catalytic behavior of the corresponded materials and the extension of the methodology in other similar materials like the CoPt/r-GO and (Fe,Co)Pd/r-GO. From the magnetic properties point of view the *fcc* to *fct* FePt transformation take place from 600 °C with very short annealing time (30 min) and the isolated FePt nanoparticles morphology give us the ability to study the FePt ordering procedure and the size effects on the magnetocrystalline anisotropy.

Notes

The authors declare no competing financial interest.

Acknowledgements

Appendix A. Supplementary data

Supplementary data related to this article can be found at http://dx.doi.org/10.1016/j.carbon.2017.05.077.

References

[1] C. Xu, X. Wang, J. Zhu, Graphene—metal particle nanocomposites, J. Phys. Chem. C 112 (2008) 19841—19845.
[2] W. Hong, H. Bai, Y. Xu, Z. Yao, Z. Gu, G. Shi, Preparation of gold nanoparticle/graphene composites with controlled weight contents and their application in biosensors, J. Phys. Chem. C 114 (2010) 1822—1826.
[3] Y. Zhang, S. Liu, W. Lu, L. Wang, J. Tian, X. Sun, In situ green synthesis of Au nanostructures on graphene oxide and their application for catalytic reduction of 4-nitrophenol, Catal. Sci. Technol. 1 (2011) 1142—1144.
[4] S. Yang, J. Dong, Z. Yao, C. Shen, X. Shi, S. Lin, et al., One-pot synthesis of graphene-supported monodisperse Pd nanoparticles as catalyst for formic acid electro-oxidation, Sci. Rep. 4 (2014) 4501.
[5] H. Joshi, K.N. Sharma, A.K. Sharma, A.K. Singh, Palladium—phosphorus/sulfur nanoparticles (NPs) decorated on graphene oxide: synthesis using the same precursor for NPs and catalytic applications in Suzuki—Miyaura coupling, Nanoscale 6 (2014) 4588—4597.
[6] C.V. Rao, C.R. Cabrera, Y. Ishikawa, Graphene-supported Pt—Au alloy nanoparticles: a highly efficient anode for direct formic acid fuel cells, J. Phys. Chem. C 115 (2011) 21963—21970.
[7] H.-K. Kim, K.C. Roh, S.-H. Park, C.-W. Lee, J.H. Jeong, S.-B. Yoon, K.-B. Kim, In situ synthesis of three-dimensional self-assembled metal oxide—reduced graphene oxide architecture, Chem. Mater. 26 (2014) 4838—4843.
[8] Z. Ji, X. Shen, Y. Xu, G. Zhu, K. Chen, Anchoring noble metal nanoparticles on CeO_2 modified reduced graphene oxide nanosheets and their enhanced catalytic properties, J. Colloid Interface Sci. 432 (2014) 57—64.
[9] Y. Sun, X. Hu, W. Luo, Y. Huang, Ultrathin CoO/graphene hybrid nanosheets: a highly stable anode material for lithium-ion batteries, J. Phys. Chem. C 116 (2012) 20794—20799.
[10] W. Fan, W. Gao, C. Zhang, W.W. Tjiu, J. Pan, T. Liu, Hybridization of graphene sheets and carbon-coated Fe_3O_4 nanoparticles as a synergistic adsorbent of organic dyes, J. Mater. Chem. 22 (2012) 25108—25115.
[11] L. Ji, M. Rao, H. Zheng, L. Zhang, Y. Li, W. Duan, J. Guo, E.J. Cairns, Y. Zhang, Graphene oxide as a sulfur immobilizer in high performance lithium/sulfur cells, J. Am. Chem. Soc. 133 (2011) 18522—18525.
[12] J. Sun, H.-W. Lee, M. Pasta, H. Yuan, G. Zheng, Y. Sun, et al., A phosphorene—graphene hybrid material as a high-capacity anode for sodium-ion batteries, Nat. Nanotechnol. 10 (2015) 980—985.
[13] Y. Yao, S. Miao, S. Liu, L.P. Ma, H. Sun, S. Wang, Synthesis, characterization, and adsorption properties of magnetic Fe_3O_4@graphene nanocomposite, Chem. Eng. J. 184 (2012) 326—332.
[14] Y. Yao, Z. Yang, D. Zhang, W. Peng, H. Sun, S. Wang, Magnetic $CoFe_2O_4$--graphene hybrids: facile synthesis, characterization, and catalytic properties, Ind. Eng. Chem. Res. 51 (2012) 6044—6051.
[15] X. Fu, Y. Liu, X. Cao, J. Jin, Q. Liu, J. Zhang, FeCo—N_x embedded graphene as high performance catalysts for oxygen reduction reaction, Appl. Catal. B Environ. 130—131 (2013) 143—151.
[16] L. Hu, R. Zhang, L. Wei, F. Zhang, Q. Chen, Synthesis of FeCo nanocrystals encapsulated in nitrogen-doped graphene layers for use as highly efficient catalysts for reduction reactions, Nanoscale 7 (2015) 450—454.
[17] S. Guo, S. Sun, FePt nanoparticles assembled on graphene as enhanced catalyst for oxygen reduction reaction, J. Am. Chem. Soc. 134 (2012) 2492—2495.
[18] D. Chen, X. Zhao, S. Chen, H. Li, X. Fu, S. Li, et al., One-pot fabrication of FePt/reduced graphene oxide composites as highly active and stable electrocatalysts for the oxygen reduction reaction, Carbon 68 (2014) 755—762.
[19] Z. Ji, G. Zhu, X. Shen, H. Zhou, C. Wu, M. Wang, Reduced graphene oxide supported FePt alloy nanoparticles with high electrocatalytic performance for methanol oxidation, New J. Chem. 36 (2012) 1774—1780.
[20] G. Wei, Y. Zhang, S. Steckbeck, Z. Su, Z. Li, Biomimetic graphene—FePt nanohybrids with high solubility, ferromagnetism, fluorescence, and enhanced electrocatalytic activity, J. Mater. Chem. 22 (2012) 17190—17195.
[21] D. Xu, Y. Tian, J. Zhao, X. Wang, High stability and reactivity of defective graphene-supported Fe_nPt_{13-n} (n = 1, 2, and 3) nanoparticles for oxygen reduction reaction: a theoretical study, J. Nanopart. Res. 17 (1) (2015) 25.
[22] X. Zheng, W. Chen, P. Cui, Z. Wang, W. Zhang, Design of multifunctional FePt/GO nanocomposites for targeting and in situ dual-modal imaging diagnostic and in situ therapeutic potential theranostic platform, RSC Adv. 4 (2014) 58489—58494.
[23] J. Kim, Y. Lee, S. Sun, Structurally ordered FePt nanoparticles and their enhanced catalysis for oxygen reduction reaction, J. Am. Chem. Soc. 132 (2010) 4996—4997.
[24] A. Capobianchi, S. Laureti, D. Fiorani, S. Foglia, E. Palange, Direct synthesis of $L1_0$ FePt nanoparticles within carbon nanotubes by wet chemical procedure, J. Phys. D. Appl. Phys. 43 (2010) 47.
[25] M. Faustini, A. Capobianchi, G. Varvaro, D. Grosso, Highly controlled dip-coating deposition of *fct* FePt nanoparticles from layered salt precursor into nanostructured thin films: an easy way to tune magnetic and optical properties, Chem. Mater. 24 (2012) 1072—1079.
[26] Aldo Capobianchi, Gaetano Campi, Mercedes Camalli, Claudio Veroli, Crystal and molecular structure of the saline complex hexaaquairon(II) hexachloroplatinate, [Fe(H$_2$O)$_6$][PtCl$_6$], Z. Krist. 224 (2009) 384—388.
[27] X.C. Hu, E. Agostinelli, C. Ni, G.C. Hadjipanayis, A. Capobianchi, A low temperature and solvent-free direct chemical synthesis of $L1_0$ FePt nanoparticles with size tailoring, Green Chem. 16 (2014) 2292—2297.
[28] Aldo Capobianchi, Marcello Colapietro, Dino Fiorani, Sabrina Foglia,

Patrizia Imperatori, Sara Laureti, Elia Palange, General strategy for direct synthesis of L1$_0$ nanoparticle alloys from layered precursor: the case of FePt, Chem. Mater. 21 (2009) 2007–2009.

[29] D.Y. Cai, M. Song, Preparation of fully exfoliated graphite oxide nanoplatelets in organic solvents, J. Mater. Chem. 17 (2007) 3678–3680.

[30] R.Y.N. Gengler, D.S. Badali, D. Zhang, K. Dimos, K. Spyrou, D. Gournis, et al., Revealing the ultrafast process behind the photoreduction of graphene oxide, Nat. Commun. 4 (2013) 1–5, 2560.

[31] V. Georgakilas, A. Demeslis, E. Ntararas, A. Kouloumpis, K. Dimos, D. Gournis, et al., Hydrophilic nanotube supported graphene–water dispersible carbon superstructure with excellent conductivity, Adv. Funct. Mater. 25 (2015) 1481–1487.

[32] C. Mattevi, G. Eda, S. Agnoli, S. Miller, K.A. Mkhoyan, O. Celik, et al., Evolution of electrical, chemical, and structural properties of transparent and conducting chemically derived graphene thin Films, Adv. Funct. Mater. 19 (2009) 2577–2583.

[33] A. Mokdad, K. Dimos, G. Zoppellaro, J. Tucek, J.A. Perman, O. Malina, et al., The non-innocent nature of graphene oxide as a theranostic platform for biomedical applications and its reactivity towards metal-based anticancer drugs, RSC Adv. 5 (2015) 76556–76566.

[34] H.-J. Shin, K.K. Kim, A. Benayad, S.-M. Yoon, H.K. Park, I.-S. Jung, et al., Efficient reduction of graphite oxide by sodium borohydride and its effect on electrical conductance, Adv. Funct. Mater. 19 (2009) 1987–1992.

[35] A.C. Ferrari, J.C. Meyer, V. Scardaci, C. Casiraghi, M. Lazzeri, F. Mauri, et al., Raman spectrum of graphene and graphene layers, Phys. Rev. Lett. 97 (2006) 187401.

[36] K.N. Kudin, B. Ozbas, H.C. Schniepp, R.K. Prud'homme, I.A. Aksay, R. Car, Raman spectra of graphite oxide and functionalized graphene sheets, Nano Lett. 8 (2008) 36–41.

[37] A. Kouloumpis, K. Spyrou, K. Dimos, V. Georgakilas, P. Rudolf, D. Gournis, A bottom-up approach for the synthesis of highly ordered fullerene-intercalated graphene hybrids, Front. Mater. 2 (10) (2015) 1–8.

[38] A. Kaniyoor, S.A. Ramaprabhu, Raman spectroscopic investigation of graphite oxide derived graphene, AIP Adv. 2 (2012), 032183.

[39] F. Torrisi, T. Hasan, W. Wu, Z. Sun, A. Lombardo, T.S. Kulmala, et al., Inkjet-printed graphene electronics, ACS Nano 6 (2012) 2992–3006.

[40] Z. Bo, X. Shuai, S. Mao, H. Yang, J. Qian, J. Chen, et al., Green preparation of reduced graphene oxide for sensing and energy storage applications, Sci. Rep. 4 (2014) 4684.

[41] S. Stankovich, D.A. Dikin, R.D. Piner, K.A. Kohlhaas, A. Kleinhammes, Y. Jia, et al., Synthesis of graphene-based nanosheets via chemical reduction of exfoliated graphite oxide, Carbon 45 (2007) 1558–1565.

[42] M.D. Stoller, S.J. Park, Y.W. Zhu, J.H. An, R.S. Ruoff, Graphene-based ultra-capacitors, Nano Lett. 8 (2008) 3498–3502.

[43] S. Zhang, X. Zhang, G. Jiang, H. Zhu, S. Guo, D. Su, et al., Tuning nanoparticle structure and surface strain for catalysis optimization, J. Am. Chem. Soc. 136 (2014) 7734–7739.

[44] S. Zhang, S. Guo, H. Zhu, D. Su, S. Sun, Structure-induced enhancement in electrooxidation of trimetallic FePtAu nanoparticles, J. Am. Chem. Soc. 134 (2012) 5060–5063.

[45] B.Y. Xia, Y. Yan, X. Wang, X.W. (David) Lou, Recent progress on graphene-based hybrid electrocatalysts, Mater. Horiz. 1 (2014) 379–399.

[46] R. Kannan, A.A. Silva, F.M. Cardoso, G. Gupta, Z. Aslam, S. Sharma, R. Steinberger-Wilckens, Study of FePt deposited reduced graphene oxide's utility as a catalyst towards oxygen reduction and methanol oxidation reactions, RSC Adv. 5 (2015) 36993–36998.